Molecular basis for enantioselective herbicide degradation imparted by aryloxyalkanoate dioxygenases in transgenic plants

Jonathan R. Chekan[a,b,1], Chayanid Ongpipattanakul[a,1], Terry R. Wright[c], Bo Zhang[d], J. Martin Bollinger Jr.[d,e], Lauren J. Rajakovich[e], Carsten Krebs[d,e], Robert M. Cicchillo[c], and Satish K. Nair[a,b,f,2]

[a]Department of Biochemistry, University of Illinois at Urbana–Champaign, Urbana, IL 61801; [b]Carl R. Woese Institute for Genomic Biology, University of Illinois at Urbana–Champaign, Urbana, IL 61801; [c]Corteva Agriscience, Agriculture Division of DowDuPont, Indianapolis, IN 46268; [d]Department of Chemistry, The Pennsylvania State University, University Park, PA 16802; [e]Department of Biochemistry and Molecular Biology, The Pennsylvania State University, University Park, PA 16802; and [f]Center for Biophysics and Quantitative Biology, University of Illinois at Urbana–Champaign, Urbana, IL 61801

Edited by Caroline S. Harwood, University of Washington, Seattle, WA, and approved May 22, 2019 (received for review January 15, 2019)

The synthetic auxin 2,4-dichlorophenoxyacetic acid (2,4-D) is an active ingredient of thousands of commercial herbicides. Multiple species of bacteria degrade 2,4-D via a pathway initiated by the Fe(II) and α-ketoglutarate (Fe/αKG)-dependent aryloxyalkanoate dioxygenases (AADs). Recently, genes encoding 2 AADs have been deployed commercially in herbicide-tolerant crops. Some AADs can also inactivate chiral phenoxypropionate and aryloxyphenoxypropionate (AOPP) herbicides, albeit with varying substrate enantioselectivities. Certain AAD enzymes, such as AAD-1, have expanded utility in weed control systems by enabling the use of diverse modes of action with a single trait. Here, we report 1) the use of a genomic context-based approach to identify 59 additional members of the AAD class, 2) the biochemical characterization of AAD-2 from *Bradyrhizobium diazoefficiens* USDA 110 as a catalyst to degrade (*S*)-stereoisomers of chiral synthetic auxins and AOPP herbicides, 3) spectroscopic data that demonstrate the canonical ferryl complex in the AAD-1 reaction, and 4) crystal structures of representatives of the AAD class. Structures of AAD-1, an (*R*)-enantiomer substrate-specific enzyme, in complexes with a phenoxypropionate synthetic auxin or with AOPP herbicides and of AAD-2, which has the opposite (*S*)-enantiomeric substrate specificity, reveal the structural basis for stereoselectivity and provide insights into a common catalytic mechanism.

herbicide | auxin | enzyme | resistance | mechanism

The phenoxyalkanoate 2,4-dichlorophenoxyacetic acid (2,4-D) is one of the oldest and most widely used systemic herbicides (1). Since its discovery during World War II by multiple groups working independently, 2,4-D has been commercialized in more than 100 countries in thousands of solo and mixture products (2, 3). In most common applications, 2,4-D is used as a selective herbicide to control a wide spectrum of broadleaf weeds in cereal crops, including corn, oats, rice, and wheat, and has uses in turf, aquatic, and pasture applications (1, 2, 4). Despite the global, long, and widespread use of 2,4-D, it remains an effective herbicide. Whereas a number of weed biotypes that are resistant to synthetic auxin herbicides have been reported (http://www.weedscience.org), few have caused significant impact, perhaps reflecting a complex mode of action of the herbicide and/or reduced fitness of some resistant biotypes (2, 5).

The bioactivity of 2,4-D derives from its structural resemblance to the plant growth hormone indole-3-acetic acid (IAA) (Fig. 1) (4). Natural auxins, such as IAA, are actively imported and exported through the actions of different transmembrane transporters (6). While 2,4-D is a substrate for the AUX1 importer, it cannot leave the cell through an exporter, and accumulation within the target results in unsustainable, disorganized cell growth and eventual plant death (7, 8). Auxins are essential for plant development and have complex downstream effects (9, 10), which likely limit the emergence of *in planta* resistance mechanisms against synthetic auxins such as 2,4-D. In contrast, several microbes from a variety of habitats have evolved pathways to degrade 2,4-D (11, 12).

Biodegradation of 2,4-D is best studied in the context of the conjugative plasmid pJP4, which allows the host bacterium (*Cupriavidus necator* JMP134) to utilize this compound as its sole carbon source (*SI Appendix*, Fig. 1) (13, 14). The catabolic cluster contains 6 genes (*tfdA–F*) (14), and initial studies identified similarities between the *tfdB–E* gene products and proteins known to enable mineralization of deschloro or monochlorinated analogs of 2,4-D (15, 16). Subsequent characterization of the *tfdA* gene product identified the enzyme as an Fe(II)- and α-ketoglutarate (αKG)-dependent dioxygenase that carries out hydroxylation of C2 in the acetate moiety of 2,4-D (17, 18). Product analyses suggested that 2,4-dichlorophenol (2,4-DCP) and glyoxylate could be spontaneously formed from this transient hemiacetal intermediate (5, 18). Further hydroxylation of 2,4-DCP by TfdB produces dichlorocatechol (19, 20), and downstream enzymes carry out intradiol ring cleavage to yield succinate as the final product

Significance

We identified dozens of hypothetical proteins that we predict to be members of the aryloxyalkanoate dioxygenase (AAD) class of enzymes that degrade both phenoxycarboxylic synthetic auxins and the aryloxyphenoxypropionate classes of herbicides. We provide a structure of a member of this class and characterize 2 AADs with opposite substrate enantioselectivities. These findings have expanded our mechanistic understanding of representative dioxygenases involved in 2,4-dichlorophenoxyacetic acid catabolism, a pathway that has been studied for nearly 40 years. The AAD enzymes, along with tolerance traits to glyphosate and glufosinate, have been successfully deployed as a component of the Enlist weed control system. This combination of herbicide and trait technology has provided tools to combat invasive weeds and to manage resistance development.

Author contributions: R.M.C. and S.K.N. designed research; J.R.C., C.O., B.Z., L.J.R., R.M.C., and S.K.N. performed research; T.R.W., B.Z., and L.J.R. contributed new reagents/analytic tools; J.R.C., C.O., B.Z., J.M.B., L.J.R., C.K., R.M.C., and S.K.N. analyzed data; and J.R.C., T.R.W., J.M.B., C.K., R.M.C., and S.K.N. wrote the paper.

The authors declare no conflict of interest.

This article is a PNAS Direct Submission.

Data deposition: The structure factors and coordinates have been deposited in the Protein Data Bank, www.wwpdb.org (PDB ID codes 5BKB–5BKE and 5BK9).

[1]J.R.C. and C.O. contributed equally to this work.

[2]To whom correspondence may be addressed. Email: snair@illinois.edu.

This article contains supporting information online at www.pnas.org/lookup/suppl/doi:10.1073/pnas.1900711116/-/DCSupplemental.

Published online June 17, 2019.

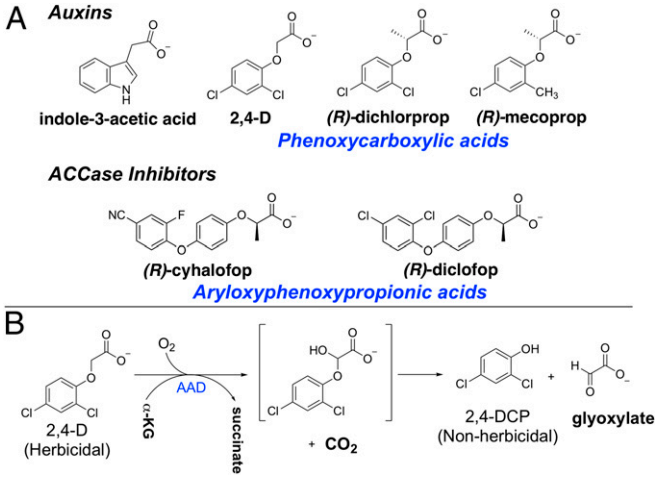

Fig. 1. Chemical structures of herbicides and the AAD catabolic pathway. (*A*) Structures of the auxin indole acetic acid and the phenoxycarboxylic synthetic analogs 2,4-D, (*R*)-dichlorprop, and (*R*)-mecoprop and the structures of the AOPP herbicides (*R*)-cyhalofop and (*R*)-diclofop. (*B*) AAD catalyzed breakdown of 2,4-D to form 2,4-DCP and glyoxylate.

(21). On the basis of the observation that 2,4-DCP has lower phytotoxicity, it was hypothesized that transgenic plants engineered with the *tfdA* gene might be resistant to the 2,4-D herbicide (22, 23). Subsequent efforts demonstrated elevated resistance to 2,4-D upon expression of *C. necator tfdA* in both tobacco (24, 25) and cotton (26).

Other phenoxycarboxylic synthetic auxins that are widely used as herbicides for broadleaf control include the chiral phenoxypropionates, dichlorprop and mecoprop (Fig. 1) (27). For both of these herbicides, only the (*R*)-enantiomers show herbicidal activity (28). Efforts to characterize homologs of TfdA with altered or expanded substrate specificity revealed sequences from the aerobic gram-negative α-proteobacterium *Sphingobium herbicidivorans* and the β-proteobacterium *Delftia acidovorans*, with 28% and 31% amino acid sequence identity to the TfdA enzyme from *C. necator* (29). Transgenic expression in monocot (maize) and dicot (soybean) crops conferred robust crop resistance over multiple generations to both the achiral phenoxyalkanoate herbicide, 2,4-D, and the chiral herbicides (5).

On the basis of sequence analysis, these TfdA homologs with activity against phenoxycarboxylic synthetic auxins were assigned the generic name AAD (for aryloxyalkanoate dioxygenase) (5). Hence, the homolog from *S. herbicidivorans* is designated as AAD-1, and the one from *D. acidovorans* is designated as AAD-12. AAD-1 has been deployed in Enlist corn (30), whereas AAD-12 confers herbicide resistance in Enlist cotton (31) and Enlist E3 soybeans (32). Neither of these AAD homologs were highly active against 2,4-D in vitro, and both had markedly diminished catalytic efficiencies (k_{cat}/K_M) relative to TfdA (~250-fold and ~10,000-fold less for AAD-12 and AAD-1, respectively [29, 33]). Nevertheless, both AAD orthologs were found to confer tolerance to 2,4-D in transgenic plants and are used for agricultural biotechnology (5).

Substrate–activity relationship studies revealed that both AAD-1 and AAD-12 can catalyze reactions that proceed with enhanced enantioselectivity (5, 29). For example, AAD-1 accepts (*R*)-dichlorprop, whereas AAD-12 has activity only against (*S*)-dichlorprop (5, 29). The expanded substrate scope of these enzymes extends beyond phenoxycarboxylic synthetic auxins, as they also carry out enantioselective cleavage of aryloxyphenoxypropionate (AOPP) herbicides. These AOPP herbicides, such as (*R*)-cyhalofop, (*R*)-diclofop, and (*R*)-quizalofop, are mechanistically distinct from the phenoxycarboxylic herbicide 2,4-D (as well as synthetic auxins from other chemical classes) (34). Specifically, the AOPPs inhibit lipid biosynthesis by targeting the monomeric acetyl-CoA carboxylases (ACCase) (35, 36). This mode of action makes the AOPPs highly selective for grasses because most dicotyledonous plants contain an additional AOPP-insensitive multimeric ACCase not present in grass species (37). Thus, AAD-1 can function as a tolerance allele against different classes of herbicides for dicot weeds (phenoxycarboxylate herbicides like 2,4-D) or grass weeds (AOPP herbicides, like (*R*)-quizalofop) (5). When deployed with other trait-enabled or naturally selective herbicides, diverse herbicide combinations can, along with other cultural practices, combat development of herbicide-resistant weeds.

Despite the agronomic importance of AAD enzymes in transgenic crops, little is known about protein–substrate interactions or how these enzymes catalyze enantioselective oxidation of herbicides. To date, no crystal structure has been reported for any member of the AAD family, and there is, therefore, an insufficient knowledge base to distinguish bona fide AADs from other enzymes of the Fe(II)/αKG dioxygenase class. In this study, we used a genomic context-based analysis to identify additional members of the AAD class. We identified AAD-2 from *Bradyrhizobium diazoefficiens* USDA 110 (44% sequence identity with TfdA) and analyzed its substrate scope and kinetic properties. We also solved the structures of 2 AADs, namely, of AAD-1 in complex with the synthetic auxin (*R*)-dichlorprop and with the AOPP herbicides (*R*)-cyhalofop and (*R*)-diclofop and of AAD-2. Structure-based analysis allowed us to identify the basis for the differing substrate scopes of AAD-2 and AAD-1.

Results and Discussion

Genome Context-Based Identification of AAD Family Members. We sought to locate other candidate AADs for further analysis to identify members that might have altered substrate selectivity. Identification of homologs is difficult using a sequence homology–based approach due to the sequence conservation with taurine dioxygenases. For example, *Escherichia coli* TauD has 30% sequence identity to TfdA, while the orthologous AAD-1 has 28% sequence identity to TfdA. We reasoned that bona fide AAD members should be genomically colocated with genes encoding downstream catabolic enzymes, including TfdB, which hydroxylates 2,4-DCP, and TfdC. Thus, to identify AADs involved in 2,4-D catabolism, we took advantage of the EFI-EST (Enzyme Function Initiative–Enzyme Similarity Tool) Sequence Similarity Network (SSN) (38) and Genome Neighborhood Network (GNN) tools (39). We found 59 putative AADs

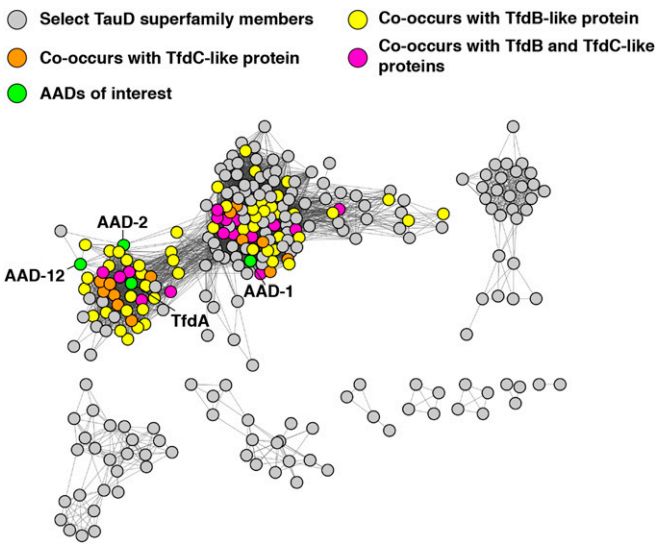

Fig. 2. Sequence similarity network of putative AAD candidates and AAD-2 substrate parameters. The EFI-EST tool was utilized to create sequence similarity networks and genome neighborhood networks for known AADs. Putative AADs were identified and consolidated with many sequences within randomly selected members of the TauD superfamily (gray nodes).

encoded within genomic contexts that also include TfdB-like and/or TfdC-like sequences (Fig. 2 and *SI Appendix*, Table S1). These pathways are overrepresented in the orders Burkholderiales, Rhodospiralles, and Rhizobiales. A phylogenetic analysis showing the relationships of the identified AADs with those previously characterized is shown as *SI Appendix*, Fig. 2.

One noteworthy point is that the canonical 2,4-D catabolic pathway in *C. necator* consists of a close clustering of TfdA with the remainder of the necessary downstream enzymes. However, this is not the case for either AAD-1 or AAD-12, which possess TfdB and TfdC homologs that are extremely distal to the TfdA-like dioxygenases (*SI Appendix*, Fig. 3). Hence, we expect that the aforementioned candidate AADs identified in our analysis represent a very conservative approximation of the true number of likely homologs. Nevertheless, we have been able to use this SSN–GNN guided approach to expand the AAD family.

Substrate Scope and Kinetic Analysis of AAD-2. The above SSN–GNN guided studies identify a number of sequences similar to TfdA that lack other 2,4-D or xenobiotic catabolic genes in close genomic proximity. To assess whether these proteins are indeed involved in 2,4-D degradation, we focused our attention on a homolog from *Bradyrhizobium diazoefficiens* USDA 110 that is 44% identical to TfdA. The presence of the corresponding gene in several bradyrhizobial strains was previously demonstrated by Southern hybridization, and the corresponding nucleotide sequence was determined using degenerate primers against *tfdA* (40). While none of these strains could catabolize 2,4-D, several showed activities toward other phenoxyacetate derivatives. In our analysis, the clustering of this sequence with AAD-12 suggests that if the corresponding enzyme were to exhibit any aryloxyalkanoate dioxygenase activity, it might also show a preference for the (*S*)-enantiomer of dichlorprop. We designated this gene *aad2* (41) and carried out biochemical studies of AAD-2 (*SI Appendix*, Fig. 4).

Examination of the substrate scope of the recombinant protein revealed that AAD-2 does indeed accept 2,4-D as a substrate. The activity of AAD-2 extends beyond 2,4-D, and the enzyme also demonstrated comparable levels of activity against the racemate and the (*S*)-enantiomer of dichlorprop but no activity against (*R*)-dichlorprop (*SI Appendix*, Fig. 5). Whereas AAD-2 showed diminished activity toward racemic compositions of the AOPP herbicide haloxyfop and fenoxaprop, no activity could be observed against (*R*)-haloxyfop. In general, the enzyme showed no activity against the (*R*)-stereoisomer of any of the phenoxycarboxylic synthetic auxin or AOPP herbicides tested. These data suggest that AAD-2 is similar to AAD-12 in that the enzyme possesses aryloxyalkanoate dioxygenase activity for chiral substrates with a strict preference for the (*S*)-stereoisomer.

To quantify the activity of AAD-2, we carried out kinetic analysis under ambient conditions using a panel of herbicide substrates (*SI Appendix*, Figs. 6 and 7). $K_{M,app}$ and $k_{cat,app}/K_{M,app}$ values of 1,100 ± 100 μM and 22 ± 2 $M^{-1}\cdot min^{-1} \times 10^2$ for 2,4-D, 1,200 ± 100 μM and 24 ± 2 $M^{-1}\cdot min^{-1} \times 10^2$ for (*S*)-dichlorprop, and 2,200 ± 400 μM and 8 ± 2 $M^{-1}\cdot min^{-1} \times 10^2$ for (*R*,*S*)-haloxyfop were measured. Additionally, (*R*,*S*)-diclofop and (*R*,*S*)-quizalofop were also tested against AAD-2; however, these compounds proved to be extremely poor substrates (*SI Appendix*, Table 2). By contrast, AAD-1 can utilize AOPP herbicides and phenoxycarboxylic auxins, including 2,4-D and (*R*)-dichlorprop, with higher catalytic efficiency (*SI Appendix*, Table 2). Even though AAD-2 can accept a range of substrates, it is a less efficient enzyme than AAD-1.

Substrate Triggering of Fe(IV)-Oxo (Ferryl) Complex Formation in the AAD-1 Reaction. The stereoselectivity of any enzyme is intimately connected to its mechanism. Several Fe/αKG dioxygenases (hydroxylases) have been studied by transient-kinetic and spectroscopic methods, and a mechanistic and kinetic paradigm has emerged (42, 43). Rapid combination of O_2 with the enzyme•Fe(II)•αKG•substrate complex (k = 10^4–10^6 $M^{-1}\cdot s^{-1}$) leads to decarboxylation of the cosubstrate and formation of a succinate-coordinated iron(IV)-oxo (ferryl) complex, which abstracts hydrogen (H•) from a carbon of the substrate. H• abstraction is often sufficiently rapid that the ferryl complex accumulates to a modest extent, if at all, but incorporation of deuterium in the scissile C–H bond of the substrate invariably slows decay of the ferryl complex (by as much as 50-fold) and allows for enhanced accumulation. Substrate hydroxylation leads to accumulation of a product complex. Product dissociation and substrate rebinding complete the cycle. For the case of the AAD-1 reaction, the expected mechanism would involve H• abstraction by the ferryl complex from the ether carbon of 2,4-D, coupling of the resultant carbon radical to the Fe(III) coordinated OH ligand (oxygen rebound), and elimination of the phenolic fragment from the unstable hemiacetal; use of 2,4-D with deuterium on the methylene carbon of the acetate moiety (d_2-2,4-D) would be expected to enhance ferryl accumulation.

To test these predictions, we carried out stopped-flow absorption experiments initiated by rapid mixing of the AAD-1•Fe(II)•αKG complex (±2,4-D) with O_2-containing buffer (Fig.

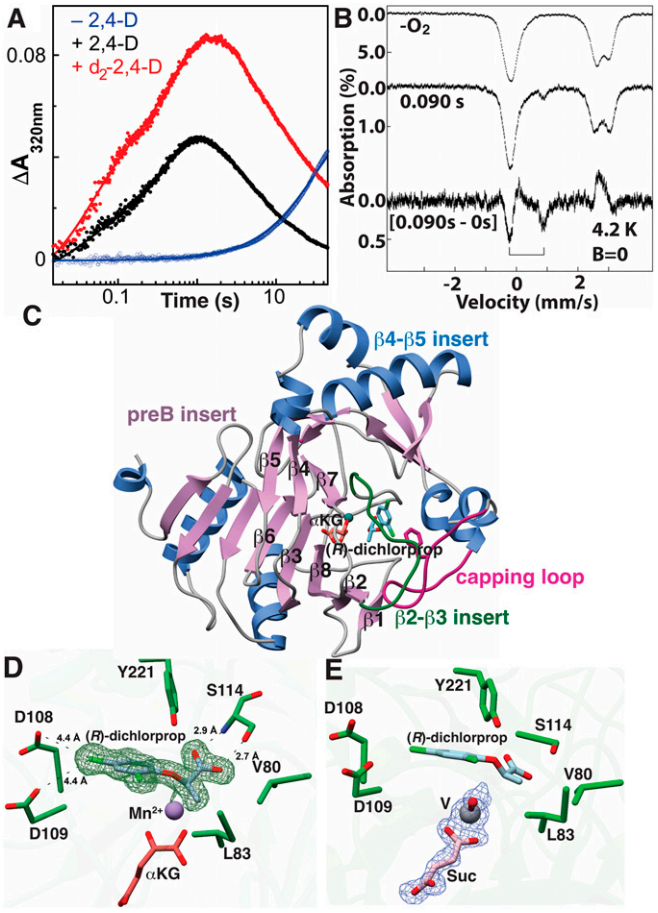

Fig. 3. Structural and functional characterization of AAD-1. (*A*) Time-dependent change in absorbance at 320 nm after mixing the AAD-1 reactant complex (±2,4-D) with O_2. (*B*) Mössbauer spectra of the reactant complex (*Top*) and a reaction sample freeze quenched near the time of maximal accumulation of the ferryl complex (0.09 s, *Middle*). The spectra were collected at 4.2 K in the absence of an externally applied magnetic field. In the difference spectrum (*Bottom*), the quadrupole doublet features of the intermediate generated upon reaction with O_2 point downward; the positions of the 2 lines are indicated by the bracket. (*C*) Ribbon diagram of AAD-1 in complex with Mn^{2+}, αKG (red), and (*R*)-dichlorprop (green). The region between β2 and β3 is indicated in green. (*D*) Active site pocket of AAD-1 in complex with bound ligands (*R*)-dichlorprop (cyan), Mn^{2+} (gray sphere), and αKG (red). The difference Fourier map ($F_o - F_c$) of (*R*)-dichlorprop is contoured at 2.5σ (green mesh). (*E*) Active site pocket of AAD-1 in complex with the vanadyl (V, gray and red) and succinate (Suc, pink). $F_o - F_c$ of vanadyl and succinate is contoured at 2.7σ (blue mesh).

3*A* and *SI Appendix*, Fig. 8). As found in other systems, reaction of the enzyme•Fe(II)•αKG ternary complex lacking the primary substrate (blue trace) is sluggish and leads to slow ($k_{obs} = 0.03\ s^{-1}$) development of ultraviolet absorption (44). In the presence of 2,4-D (black trace), a more rapid, biphasic ($k_{obs} \sim 30, 2\ s^{-1}$) increase in absorption signifies "triggering" of O_2 reactivity by the binding of the substrate, a phenomenon previously attributed to dissociation of a water ligand from the Fe(II) cofactor (45, 46). The developing absorption is transient (k_{obs} for decay of ~0.4, 0.07 s^{-1}), suggesting that it could arise from the canonical ferryl intermediate. The corresponding trace from the reaction with d_2-2,4-D (red trace) shows increased transient absorption, consistent with enhanced accumulation of the H•-abstracting ferryl complex (47). However, the overall enhancement by deuterium substitution is less profound (total rise phase amplitude of ~0.12 compared with ~0.08) than would be anticipated were the original absorbance change at 320 nm vs. time trace to reflect solely development and decay of the ferryl complex. The rise phase is even more obviously biphasic (k_{obs} of 25 and 2 s^{-1}) with the deuterium-labeled substrate than with the protium-containing substrate and has almost 3 times the amplitude in the fast phase (0.046 compared with 0.017), suggesting that the effect of deuterium is largely in this first, fast phase. Indeed, the results of parallel freeze–quench Mössbauer experiments imply that only this phase reflects accumulation of the ferryl complex. Mössbauer spectra of reaction samples freeze quenched at different times reveal the development of a quadrupole doublet with parameters (isomer shift $\delta = 0.31$ mm/s and quadrupole splitting parameter $|\Delta E_Q| = 1.15$ mm/s; Fig. 3*B*) that are typical of high-spin ferryl intermediates observed in other mononuclear non-heme-iron enzymes (42, 43). Importantly, this quadrupole doublet is present in the spectrum of the 0.090 s sample but absent in the spectra of the reactant complex and the 0.280 s sample, implying that it is associated with an intermediate that accumulates in the fast rise phase observed in the stopped-flow experiments (*SI Appendix*, Fig. 9). Evidence for the canonical ferryl complex as an intermediate in the AAD-1 reaction provides the mechanistic basis for the crystallographic studies described in *Structural Basis for Broad Herbicide Tolerance of AAD-1*.

Structural Basis for Broad Herbicide Tolerance of AAD-1. We determined crystal structures of AAD-1 in complex with Mn^{2+}, αKG, and either (*R*)-dichlorprop (1.58 Å resolution), (*R*)-cyhalofop (1.9 Å resolution), or (*R*)-diclofop (1.8 Å resolution). To provide the most direct link to the reaction mechanism, we also solved a 1.51 Å resolution structure of AAD-1 in complex with succinate, (*R*)-dichlorprop, and the vanadyl (vanadium(IV)-oxo) mimic of the ferryl intermediate (48, 49). These structures reveal the basis for the broad substrate tolerance of AAD-1. Last, we determined the 2.15 Å resolution structure of the AAD-2•Mn^{2+}•*N*-oxalylglycine (NOG) ternary complex, which, by comparison with the structures of AAD-1, is informative regarding their differing stereoselectivities. Crystallographic phases were determined by molecular replacement using the coordinates of the TauD (Protein Data Bank [PDB] Code 1GQW, 30% sequence identity) (50).

AAD-1 has the double-stranded β-helix (DSBH) fold found in other members of the Fe/αKG oxygenase family (43, 51), with *E. coli* TauD being the closest structural homolog (rmsd of 1.8 Å over 269 aligned Cαs) (50). The enzyme crystallized as a dimer in the crystallographic asymmetric unit and Mn^{2+} and αKG were present in both active sites (Fig. 3*C*). As in the structure of TauD (50), insertions between strands β4 and β5, relative to the DSBH fold, contribute to the dimerization interface. In the AAD-1 structure, a facial triad consisting of His111, His270, and Asp113 coordinates the catalytic metal ion (52). The αKG interacts with the metal in a bidentate manner, the C1 and the C5 carboxylates form hydrogen bonds with Arg285 and Arg281, respectively.

Notably, electron density was observed for the herbicide in 1 of 2 monomers, which also shows continuous features for the substrate-capping loop. Prior structures of other Fe/αKG enzymes have shown that the substrate-capping loop becomes ordered only upon binding of the substrate in the active site. In the structure of AAD-1, the equivalent loop is larger and consists of a long, extended loop between Ser183 through Asp193, and several residues in this loop are in contact with the bound substrate. Most notably, Phe182 is in contact with the phenoxypropionate ring of the substrate and forms a closed hydrophobic pocket (Fig. 3*C*).

The structures of the Mn(II)•αKG•(*R*)-dichlorprop and vanadyl•succinate•(*R*)-dichlorprop complexes of AAD-1 represent mimics of its reactant and ferryl-intermediate states, respectively (Fig. 3 *D* and *E*). In each of these structures, the substrate is proximal to the metal and is engaged by electrostatic interactions and hydrophobic packing. The carboxylic acid of (*R*)-dichlorprop is within hydrogen-bonding distance of both the side chain and backbone nitrogen of Ser114, while the *p*-chloro atom is within halogen-bonding distance of Asp108 and Asp109. Prior modeling studies based on TauD predicted binding of the ligand in an extended orientation (53), while our structural data show that (*R*)-dichlorprop binds in a bent conformation that directs the phenoxy ring toward a solvent-exposed opening.

The vanadyl ion was previously shown to mimic the ferryl (Fe(IV)-oxo) complex in other Fe/αKG oxygenases (48, 49). In the AAD-1–vanadyl•succinate structure, the oxo ligand is positioned appropriately for abstraction of H• from the substrate, whereas the methyl group of the chiral substrate is held within a hydrophobic pocket composed of Val80, Leu83, Ile95, and Ile106. The resultant Fe(III)-hydroxo species would then rebound onto the carbon-centered substrate radical to generate the hemiacetal intermediate. The V-oxo bond distance is 1.88 Å, which is longer than the values of 1.58–1.63 Å reported for model compounds and likely reflects photoreduction of the vanadium (IV) upon exposure to X-rays, as observed in other systems (49).

The cocrystal structures with (*R*)-diclofop and (*R*)-cyhalofop provide the basis for understanding the substrate tolerance of AAD-1 against the AOPP class of grass-specific herbicides. AOPPs have scaffolds that are similar to that of phenoxycarboxylic synthetic auxins but contain an additional aromatic ring attached to the phenoxy moiety. Both (*R*)-diclofop and (*R*)-cyhalofop bind at the AAD-1 active site in a manner similar to that of the phenoxycarboxylic synthetic auxin, with their chiral carbon oriented directly above the metal and the methyl group projecting into the aforementioned hydrophobic pocket (Fig. 4 *A* and *B*). The additional aryl rings of both (*R*)-diclofop and (*R*)-cyhalofop are accommodated within a solvent-exposed tunnel comprising Arg104, Asp108, Asp109, Val170, Phe182, and Val220. There are limited interactions between the extended ring of these AOPP herbicides and residues in AAD-1, and only Val220 makes van der Waals contacts with the ring. A superposition of these structures with that of AAD-1 bound to the smaller (*R*)-dichlorprop reveals that enzyme residues Arg104, Asp109, and Gln219 shift away from the tunnel to accommodate the second ring. The presence of this solvent-exposed tunnel was not evident in earlier modeling studies

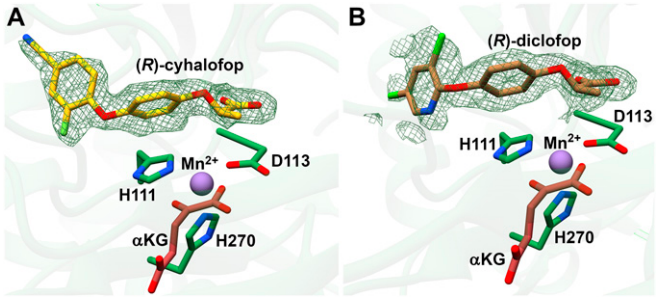

Fig. 4. Substrate-binding pocket of AAD-1 with bound AOPPs. (*A*) Active site pocket of AAD-1 in complex with (*R*)-cyhalofop, Mn^{2+}, and αKG. (*B*) Active site pocket of AAD-1 in complex with (*R*)-diclofop, Mn^{2+}, and αKG. $F_o - F_c$ of each AOPP is contoured to 2.5σ.

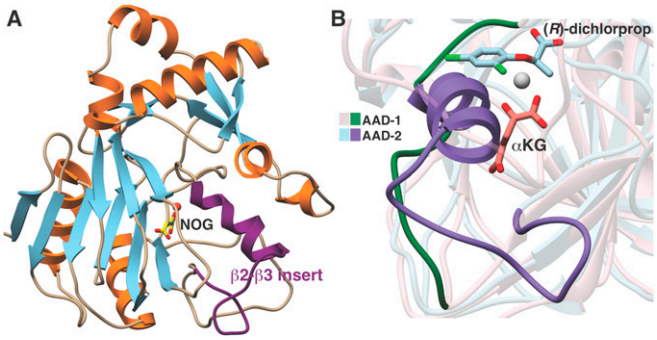

Fig. 5. Crystal structure and structure-based sequence alignment of AAD-2. (*A*) Ribbon diagram of the AAD-2–NOG (yellow) complex, highlighting the β2–β3 helical insert (purple). (*B*) Close-up of the AAD-1–(*R*)-dichlorprop substrate pocket superimposed onto the AAD-2 structure. The β2–β3 helical insert obstructs binding of the (*R*)-enantiomers of herbicides.

(50). The lack of significant interactions between residues in the tunnel and the AOPP herbicides suggests that AAD-1 also may be able to degrade other molecules based on the (*R*)-dichlorprop scaffold (with an aryloxyalkanoate moiety) (5, 41).

Basis for Substrate Enantioselectivity. A notable feature of AAD-2 is the altered substrate enantioselectivity, as this enzyme is able to process only the (*S*)-stereoisomer of the chiral phenoxycarboxylic auxins and AOPP herbicides. To understand the basis for this switch in stereospecificity, we determined the 2.15 Å resolution crystal structure of AAD-2 in complex with Mn^{2+} and the αKG mimic NOG (Fig. 5*A*). The overall structure of AAD-2 recapitulates features common to other Fe/αKG oxygenases (51). The crystal structures of AAD-1 and AAD-2 can be superimposed with a rmsd value of 2.8 Å over 256 aligned Cα atoms, illustrative of a strong conservation of the overall folds, despite only 29% sequence identity between the 2 proteins. A facial triad of His155, Asp117, and His264 coordinates the metal ion, with NOG binding to the metal in a bidentate fashion. The NOG also engages in hydrogen bonds with Arg275 and Arg279. While (*S*)-dichlorprop was included in the crystallization media, density for the bound ligand was not evident.

The superposition of the AAD-2 structure with that of AAD-1/(*R*)-dichlorprop provides insights into the enantioselectivity of AAD-2. Although the overall structures align fairly well, there are significant differences in the loops that connect strands β2 and β3 (Fig. 5*B*). Prior structure-based analysis supports a role for this so-called β2/β3 loop in substrate binding (51), and the differences between AAD-1 and AAD-2 are the result of an ∼20-residue insertion in the loop region of the latter. This insertion consists of residues Asn90 through Cys112 in AAD-2, and its structure is partially stabilized by the formation of a short α-helix by residues Leu108 through Asn111. In the AAD-2 structure, this helix would sterically clash with the orientation of (*R*)-dichlorprop observed in the AAD-1 structure, necessitating a different substrate-binding pose, which likely results in the change in substrate stereospecificity. This insertion is also evident in the sequence of AAD-12 and TfdA, accounting for the (*S*)-stereospecificity of the enzymes (*SI Appendix*, Fig. 10).

A second distinguishing structural feature of AAD-2 is its shorter substrate-capping loop in comparison with that in AAD-1. In general, each of the (*S*)-specific AADs has a substrate-capping loop that is shortened by 4 to 10 residues in the region surrounding and including Ser183 through Asp193 (*SI Appendix*, Fig. 10). In AAD-1 structure, residues in the extended substrate-capping loop are in van der Waals contact with the substrate, and Phe182 in the loop is positioned for hydrophobic interactions with the phenoxypropionate ring in the substrate tunnel. Changes in both the length and identity of residues in this loop may result in differences in enantioselectivity among AADs.

Conclusion

Genes involved in the microbial degradation pathway for 2,4-D were identified nearly 4 decades ago, but insights into the structure–function relationships within the aryloxyalkanoate dioxygenase family have been lacking. Here, we have used a multidisciplinary approach to shed light on AADs, including the identification of 59 members of this family and detailed characterization of one such representative, specifically, AAD-2. High-resolution cocrystal structures of AAD-1 and AAD-2, along with kinetic and spectroscopic analyses, provide insights into both the reaction mechanism and the basis for enantiospecificity.

One noteworthy outcome of this study is that, thus far, AAD-1 is the only characterized member that shows substrate specificity for the (*R*)-enantiomer, while members with the opposite (*S*) enantiospecificity are more prevalent (namely, AAD-2 and AAD-12, among others). One plausible explanation for this seeming overrepresentation of (*S*)-type AADs is that when dichlorprop was first marketed in the 1960s, it was commercially available as the racemate. Hence, while the bioactive (*R*)-dichlorprop was imported into target broadleaf weeds, the accumulation of the (*S*)-dichlorprop in soil samples may have facilitated evolution of biosynthetic pathways for the catabolism of only this enantiomer. While advances in asymmetric synthesis long ago made possible the commercialization of enantiomerically pure herbicides, the AADs that catabolize the (*S*)-enantiomers still reside in the microbiome. An equally plausible reason for the abundance of (*S*)-type AADs is that their natural substrates may be an as-yet-unidentified (*S*)-phenoxypropionate metabolite that is present in soil microenvironments. The natural substrates for either the (*R*)- or (*S*)-type AADs are not currently known.

AAD-1-transformed corn is now being marketed under the trade name Enlist and is currently being deployed with 2 additional herbicide-tolerant traits (to glyphosate and glufosinate) along with multiple insect control traits as corn products known as SmartStax Enlist. Transgenic plants containing AAD-1 simultaneously show robust tolerance to 2,4-D in corn (already partially tolerant) and to (*R*)-quizalofop (normally lethal to corn). These herbicides are now deployed in combination treatments with broad-spectrum herbicides such as glyphosate or glufosinate, allowing farmers to flexibly control targeting of both broadleaf and grass weeds using herbicides that have multiple modes of action. When used in an integrated weed management system, diversifying herbicide modes of action with additional trait-enabled herbicide chemistries is expected to slow development of weed resistance and help sustain effective weed control tools (30).

Materials and Methods

Protocols for AAD expression and purification, AAD-1 activity under conditions of stopped flow and freeze–quench experiments, and determination of AAD-2 kinetic parameters and substrate scope, can be found in the *SI Appendix*. The structure factors and coordinates have been deposited in the Protein Data Bank (accession IDs 5BKB [AAD-1 with (*R*)-dichlorprop]; 5BKD [AAD1 with (*R*)-cyhalofop]; 5BKC [AAD-1 with (*R*)-diclofop]; 5BK9 [AAD-1 with vanadyl]; and 5BKE [AAD-2]).

Structure Determination of AAD-1 and AAD-2. All data were collected at Argonne National Laboratory (Lemont, IL) at Sector 21 Life Sciences–Collaborative Access Team and the AAD-2 data collected at Sector 19 Structural Biology Center–Collaborative Access Team. The autoPROC software package (54) was utilized for indexing and scaling of the diffraction data. Initial phases for both AAD-1 and AAD-2 were obtained using PHASER (55) as implemented in the PHENIX software package (56) using the coordinates of TauD (PDB Code 1GQW) as a search model. Initial models were built using PHENIX and Parrot/Buccaneer (57). Manual refinements were completed by the iterative use of COOT (58) and phenix.refine (59). Cross validation was utilized throughout the model-building process to monitor building bias (60). The stereochemistry of all of the models was routinely monitored using PROCHECK (61). Crystallographic statistics are provided in *SI Appendix*, Table S3.

ACKNOWLEDGMENTS. This work was supported in part by the NIH (award GM-69657 to J.M.B. and C.K. and award GM-127079 to C.K.). We thank Dr. Joshua Roth of Corteva Agriscience for providing d_2-2,4-D.

1. R. Pohanish, *Sittig's Handbook of Pesticides and Agricultural Chemicals* (Elsevier, New York, 2015).
2. R. Busi *et al*., Weed resistance to synthetic auxin herbicides. *Pest Manag. Sci.* **74**, 2265–2276 (2018).
3. M. A. Peterson, S. A. McMaster, D. E. Riechers, J. Skelton, P. W. Stahlman, 2,4-D past, present, and future: A review. *Weed Technol.* **30**, 303–345 (2015).
4. Y. Song, Insight into the mode of action of 2,4-dichlorophenoxyacetic acid (2,4-D) as an herbicide. *J. Integr. Plant Biol.* **56**, 106–113 (2014).
5. T. R. Wright *et al*., Robust crop resistance to broadleaf and grass herbicides provided by aryloxyalkanoate dioxygenase transgenes. *Proc. Natl. Acad. Sci. U.S.A.* **107**, 20240–20245 (2010).
6. K. Fukui, K. I. Hayashi, Manipulation and sensing of auxin metabolism, transport and signaling. *Plant Cell Physiol.* **59**, 1500–1510 (2018).
7. M. J. Bennett *et al*., Arabidopsis AUX1 gene: A permease-like regulator of root gravitropism. *Science* **273**, 948–950 (1996).
8. K. Hoyerova *et al*., Auxin molecular field maps define AUX1 selectivity: Many auxin herbicides are not substrates. *New Phytol.* **217**, 1625–1639 (2018).
9. W. A. Peer, From perception to attenuation: Auxin signalling and responses. *Curr. Opin. Plant Biol.* **16**, 561–568 (2013).
10. H. Vogler, C. Kuhlemeier, Simple hormones but complex signalling. *Curr. Opin. Plant Biol.* **6**, 51–56 (2003).
11. R. R. Fulthorpe, C. McGowan, O. V. Maltseva, W. E. Holben, J. M. Tiedje, 2,4-Dichlorophenoxyacetic acid-degrading bacteria contain mosaics of catabolic genes. *Appl. Environ. Microbiol.* **61**, 3274–3281 (1995).
12. T. K. Nielsen *et al*., Evolution of sphingomonad gene clusters related to pesticide catabolism revealed by genome sequence and mobilomics of Sphingobium herbicidovorans MH. *Genome Biol. Evol.* **9**, 2477–2490 (2017).
13. R. H. Don, J. M. Pemberton, Properties of six pesticide degradation plasmids isolated from Alcaligenes paradoxus and Alcaligenes eutrophus. *J. Bacteriol.* **145**, 681–686 (1981).
14. R. H. Don, A. J. Weightman, H. J. Knackmuss, K. N. Timmis, Transposon mutagenesis and cloning analysis of the pathways for degradation of 2,4-dichlorophenoxyacetic acid and 3-chlorobenzoate in Alcaligenes eutrophus JMP134(pJP4). *J. Bacteriol.* **161**, 85–90 (1985).
15. E. J. Perkins, M. P. Gordon, O. Caceres, P. F. Lurquin, Organization and sequence analysis of the 2,4-dichlorophenol hydroxylase and dichlorocatechol oxidative operons of plasmid pJP4. *J. Bacteriol.* **172**, 2351–2359 (1990).
16. J. R. van der Meer, W. M. de Vos, S. Harayama, A. J. Zehnder, Molecular mechanisms of genetic adaptation to xenobiotic compounds. *Microbiol. Rev.* **56**, 677–694 (1992).
17. F. Fukumori, R. P. Hausinger, Alcaligenes eutrophus JMP134 "2,4-dichlorophenoxyacetate monooxygenase" is an alpha-ketoglutarate-dependent dioxygenase. *J. Bacteriol.* **175**, 2083–2086 (1993).
18. F. Fukumori, R. P. Hausinger, Purification and characterization of 2,4-dichlorophenoxyacetate/alpha-ketoglutarate dioxygenase. *J. Biol. Chem.* **268**, 24311–24317 (1993).
19. L. Farhana, P. B. New, The 2,4-dichlorophenol hydroxylase of Alcaligenes eutrophus JMP134 is a homotetramer. *Can. J. Microbiol.* **43**, 202–205 (1997).
20. T. Ledger, D. H. Pieper, B. González, Chlorophenol hydroxylases encoded by plasmid pJP4 differentially contribute to chlorophenoxyacetic acid degradation. *Appl. Environ. Microbiol.* **72**, 2783–2792 (2006).
21. A. Kumar, N. Trefault, A. O. Olaniran, Microbial degradation of 2,4-dichlorophenoxyacetic acid: Insight into the enzymes and catabolic genes involved, their regulation and biotechnological implications. *Crit. Rev. Microbiol.* **42**, 194–208 (2016).
22. E. J. Perkins, C. Stiff, P. F. Lurquin, Use of alcaligenes eutrophus as a source of genes for 2,4-D resistance in plants. *Weed Sci.* **35**, 12–18 (1987).
23. S. G. Taylor, D. G. Schilling, K. H. Quesenberry, G. R. Chaudhry, Phytotoxicity of 2,4-D and 2,4-dichlorophenol to red clover (Trifolium pratense). *Weed Sci.* **37**, 825–829 (1989).
24. B. R. Lyon, D. J. Llewellyn, J. L. Huppatz, E. S. Dennis, W. J. Peacock, Expression of a bacterial gene in transgenic tobacco plants confers resistance to the herbicide 2,4-dichlorophenoxyacetic acid. *Plant Mol. Biol.* **13**, 533–540 (1989).
25. W. R. Streber, L. Willmitzer, Transgenic tobacco plants expressing a bacterial detoxifying enzyme are resistant to 2,4-D. *Nat. Biotechnol.* **7**, 811–816 (1989).
26. C. Bayley *et al*., Engineering 2,4-D resistance into cotton. *Theor. Appl. Genet.* **83**, 645–649 (1992).
27. M. Quareshy, J. Prusinska, J. Li, R. Napier, A cheminformatics review of auxins as herbicides. *J. Exp. Bot.* **69**, 265–275 (2018).
28. M. Matell, Stereochemical studies on plant growth regulators. VII. Optically active α-(2-methyl-4-chlorophenoxy)-propionic acid and α-(2,4-dichlorophenoxy)-n-butyric acid and their steric relations. *Ark. Kemi* **6**, 365–373 (1953).
29. T. A. Müller, T. Fleischmann, J. R. van der Meer, H. P. Kohler, Purification and characterization of two enantioselective alpha-ketoglutarate-dependent dioxygenases, RdpA and SdpA, from Sphingomonas herbicidovorans MH. *Appl. Environ. Microbiol.* **72**, 4853–4861 (2006).
30. D. C. Ruen *et al*., Tolerance of corn with glyphosate resistance and the aryloxyalkanoate dioxygenase trait (AAD-1) to 2,4-D choline and glyphosate. *Weed Technol.* **31**, 217–224 (2017).
31. L. B. Braxton *et al*., Resistance of Enlist (AAD-12) cotton to glufosinate. *Weed Technol.* **31**, 380–386 (2017).
32. R. L. Frene *et al*., Enlist E3 soybean sensitivity and enlist herbicide-based program control of sumatran fleabane (Conyza sumatrensis). *Weed Technol.* **32**, 416–423 (2018).
33. K. Nickel, M. J. Suter, H. P. Kohler, Involvement of two alpha-ketoglutarate-dependent dioxygenases in enantioselective degradation of (R)- and (S)-mecoprop by Sphingomonas herbicidovorans MH. *J. Bacteriol.* **179**, 6674–6679 (1997).
34. S. B. Powles, Q. Yu, Evolution in action: Plants resistant to herbicides. *Annu. Rev. Plant Biol.* **61**, 317–347 (2010).
35. J. Secor, C. Cséke, Inhibition of acetyl-CoA carboxylase activity by haloxyfop and tralkoxydim. *Plant Physiol.* **86**, 10–12 (1988).
36. W. G. Whittingham, *Herbicidal Aryloxyphenoxypropionate Inhibitors of Acetyl-CoA Carboxylase* (Wiley-VCH, 2016).
37. K. K. Hatzios, *Cases and Mechanisms of Resistance to ACCase-Inhibiting Herbicides* (American Chemical Society, 2002).
38. J. A. Gerlt *et al*., Enzyme function initiative-enzyme similarity tool (EFI-EST): A web tool for generating protein sequence similarity networks. *Biochim. Biophys. Acta* **1854**, 1019–1037 (2015).
39. J. A. Gerlt, Genomic enzymology: Web tools for leveraging protein family sequence-function space and genome context to discover novel functions. *Biochemistry* **56**, 4293–4308 (2017).
40. K. Itoh *et al*., Root nodule Bradyrhizobium spp. harbor tfdAalpha and cadA, homologous with genes encoding 2,4-dichlorophenoxyacetic acid-degrading proteins. *Appl. Environ. Microbiol.* **70**, 2110–2118 (2004).
41. T. R. Wright, J. M. Lira, D. Merlo, N. L. Arnold, "Herbicide resistance genes." US Patent 7838733 (2010).
42. J. M. Bollinger Jr. *et al*., "Mechanisms of 2-oxoglutarate-dependent oxygenases: The hydroxylation paradigm and beyond" in *2-Oxoglutarate-Dependent Oxygenases*, C. J. Schofield, R. P. Hausinger, Eds. (Royal Society of Chemistry, London, 2015), pp. 95–122.
43. C. Krebs, D. Galonić Fujimori, C. T. Walsh, J. M. Bollinger Jr., Non-heme Fe(IV)-oxo intermediates. *Acc. Chem. Res.* **40**, 484–492 (2007).
44. M. L. Matthews *et al*., Substrate-triggered formation and remarkable stability of the C-H bond-cleaving chloroferryl intermediate in the aliphatic halogenase, SyrB2. *Biochemistry* **48**, 4331–4343 (2009).
45. E. I. Solomon *et al*., Geometric and electronic structure/function correlations in non-heme iron enzymes. *Chem. Rev.* **100**, 235–350 (2000).
46. J. Zhou *et al*., Spectroscopic studies of substrate interactions with clavaminate synthase 2, a multifunctional alpha-KG-dependent non-heme iron enzyme: Correlation with mechanisms and reactivities. *J. Am. Chem. Soc.* **123**, 7388–7398 (2001).
47. J. M. Bollinger Jr., C. Krebs, Stalking intermediates in oxygen activation by iron enzymes: Motivation and method. *J. Inorg. Biochem.* **100**, 586–605 (2006).
48. R. J. Martinie *et al*., Vanadyl as a stable structural mimic of reactive ferryl intermediates in mononuclear nonheme-iron enzymes. *Inorg. Chem.* **56**, 13382–13389 (2017).
49. A. J. Mitchell *et al*., Visualizing the reaction cycle in an iron(II)- and 2-(oxo)-glutarate-dependent hydroxylase. *J. Am. Chem. Soc.* **139**, 13830–13836 (2017).
50. J. M. Elkins *et al*., X-ray crystal structure of Escherichia coli taurine/alpha-ketoglutarate dioxygenase complexed to ferrous iron and substrates. *Biochemistry* **41**, 5185–5192 (2002).
51. W. Aik, M. A. McDonough, A. Thalhammer, R. Chowdhury, C. J. Schofield, Role of the jelly-roll fold in substrate binding by 2-oxoglutarate oxygenases. *Curr. Opin. Struct. Biol.* **22**, 691–700 (2012).
52. K. D. Koehntop, J. P. Emerson, L. Que , Jr., The 2-His-1-carboxylate facial triad: A versatile platform for dioxygen activation by mononuclear non-heme iron(II) enzymes. *J. Biol. Inorg. Chem.* **10**, 87–93 (2005).
53. T. A. Müller, M. I. Zavodszky, M. Feig, L. A. Kuhn, R. P. Hausinger, Structural basis for the enantiospecificities of R- and S-specific phenoxypropionate/alpha-ketoglutarate dioxygenases. *Protein Sci.* **15**, 1356–1368 (2006).
54. C. Vonrhein *et al*., Data processing and analysis with the autoPROC toolbox. *Acta Crystallogr. D Biol. Crystallogr.* **67**, 293–302 (2011).
55. A. J. McCoy, Solving structures of protein complexes by molecular replacement with Phaser. *Acta Crystallogr. D Biol. Crystallogr.* **63**, 32–41 (2007).
56. T. C. Terwilliger *et al*., phenix.mr_rosetta: Molecular replacement and model rebuilding with Phenix and Rosetta. *J. Struct. Funct. Genomics* **13**, 81–90 (2012).
57. K. Cowtan, The Buccaneer software for automated model building. 1. Tracing protein chains. *Acta Crystallogr. D Biol. Crystallogr.* **62**, 1002–1011 (2006).
58. P. Emsley, B. Lohkamp, W. G. Scott, K. Cowtan, Features and development of Coot. *Acta Crystallogr. D Biol. Crystallogr.* **66**, 486–501 (2010).
59. T. C. Terwilliger *et al*., Iterative model building, structure refinement and density modification with the PHENIX AutoBuild wizard. *Acta Crystallogr. D Biol. Crystallogr.* **64**, 61–69 (2008).
60. A. T. Brünger *et al*., Crystallography & NMR system: A new software suite for macromolecular structure determination. *Acta Crystallogr. D Biol. Crystallogr.* **54**, 905–921 (1998).
61. R. A. Laskowski, J. A. Rullmannn, M. W. MacArthur, R. Kaptein, J. M. Thornton, AQUA and PROCHECK-NMR: Programs for checking the quality of protein structures solved by NMR. *J. Biomol. NMR* **8**, 477–486 (1996).